CrossMark

RESEARCH PAPER

Flexural wave propagation in fluid-conveying carbon nanotubes with system uncertainties

Hu Liu[1] · Zheng Lv[1] · Qi Li[2]

© Springer-Verlag GmbH Germany 2017

Abstract Many studies have reported that the material properties of carbon nanotubes (CNTs) show a wide range and exhibit a great of uncertainties. The uncertainty, in turn, will affect the physical behaviors of CNTs. In this paper, an iterative algorithm-based interval analysis method is proposed to deal with the flexural wave propagation characteristics of fluid-conveying CNTs with system uncertainties. To make the conclusion more objective, the properties of the material and fluid are all considered as uncertain-but-bounded parameters, which can effectively describe the uncertainties where few data are available to perform the probabilistic analysis. The upper and lower bounds of the wave dispersion curves are predicted to clarify the influences of the uncertain material and fluid properties on the wave propagation behaviors of fluid-conveying CNTs. It is demonstrated that the widths of the wave frequency and phase velocity behave different at different wavelengths. Besides, the bounds predicted by the probabilistic model are given to verify the present model, and the present model is also validated by comparing with the Monte Carlo simulation. The present model provides some useful guides for using CNTs to convey fluid flows.

✉ Zheng Lv
  lvbaolvzheng@buaa.edu.cn

[1] Institute of Solid Mechanics, Beihang University, Beijing 100191, People's Republic of China

[2] State Key Laboratory of Robotics, Shenyang Institute of Automation, Chinese Academy of Sciences, Shenyang 110016, Liaoning, People's Republic of China

1 Introduction

Carbon nanotubes (CNTs), discovered by Iijima (1991), have exhibited outstanding application prospects in nanodevice, nanoelectronics, and nanocomposite due to their remarkable physical, mechanical, electrical, thermal, and optical properties (Mattia and Gogotsi 2008). It is essential to understand the physical and mechanical behaviors of CNTs for better guiding its applications in engineering. However, the small size effect of CNTs brings two challenges to the research.

One problem is that the traditional theories and methods will lose effectiveness. Although the molecular dynamic (MD) simulation is widely accepted as an effective method to reflect the size-dependent mechanical behaviors of CNTs, this method is limited to structures with a small number of atoms, and it is also time consuming. In this case, an efficient continuum theory is needed to account for the size-dependent effect of CNTs. Unfortunately, the classical continuum theory is no longer applicable to capture the small-scale effects of CNTs due to the lack of size-scale parameter (Ansari et al. 2015; Li et al. 2016). Recently, the nonlocal continuum theory, which assumes that the stress tensor at any point is dependent on the whole strain field of the continuum, is widely used to characterize the small-scale effects of CNTs. This theory was firstly proposed by Eringen (1972) and was successfully used in solving the vibration (De Rosa and Lippiello 2017; Deng and Yang 2014; Ebrahimi and Nasirzadeh 2015; Hu et al. 2012; Kiani 2013a, b; Xia and Wang 2010; Zhen et al. 2011), wave propagation (Aydogdu 2014; Huang et al. 2013; Narendar and Gopalakrishnan 2010; Narendar et al. 2012; Wang et al. 2006, 2013, 2015), and buckling (Adali 2008; Amara et al. 2010; Khademolhosseini et al. 2010; Robinson and Adali 2016; Setoodeh et al.

2011) problems of CNTs. Several different nonlocal continuum theories, such as the nonlocal Euler–Bernoulli beam (Setoodeh et al. 2011; Wang et al. 2015; Zhen et al. 2011), nonlocal Timoshenko beam (De Rosa and Lippiello 2017; Narendar and Gopalakrishnan 2010; Xia and Wang 2010), and nonlocal shell (Khademolhosseini et al. 2010) theory, were adopted to study the mechanical behaviors of CNTs, in particular, because the CNT comprises a sheet of carbon atoms, which makes it perfect a candidate for nanocontainers to store gases and for nanotubes to convey fluids (Ansari et al. 2016; Bahaadini and Hosseini 2016; Li et al. 2016; SafarPour and Ghadiri 2017). Several different types of fluids such as water (Hanasaki and Nakatani 2006; Mattia and Calabrò 2012; Zhang et al. 2010), methane, ethane, and ethylene molecules (Mao and Sinnott 2000) and light gases (Skoulidas et al. 2002) were reported by many researchers. In this case, the effects of the conveying fluids on mechanical behaviors of CNTs have aroused worldwide academic interests (Mattia and Gogotsi 2008). For instance, Narendar and Gopalakrishnan (2010) proposed a nonlocal Timoshenko beam model to investigate the terahertz wave propagation behavior in fluid-conveying single-walled CNTs. Based on nonlocal Euler–Bernoulli beam theory, Bahaadini and Hosseini (2016) analyzed the divergence and flutter instability of fluid-conveying CNTs under combined effect of elastic foundation and magnetic field. Kiani (2013b) studied the vibration behavior of CNTs subjected to an inside viscous fluid flow by using Eringen's nonlocal elasticity theory. Other similar analyses also can be found in Refs. (Abbasnejad et al. 2015; Amiri et al. 2016; Chang 2013a, b; Deng and Yang 2014; Wang et al. 2013; Xia and Wang 2010).

The other problem induced by the small size effect is that the uncertainties during the nanoscale system will become much more serious. The model inaccuracies, physical imperfections, material defects, and system complexities are unavoidable, and they both would introduce system uncertainties. Many experimental results have indicated that the Young's modulus of CNTs has a wide range and shows a great of uncertainties. For instance, Salvetat et al. (1999) used an atomic force microscope experiment to measure the flexural Young's modulus and shear modulus of CNTs, and 50% of error was found in their test results. Krishnan et al. (1998) measured 27 CNTs and found that the Young's modulus was in a wide range of 1.3–0.4/+0.6 TPa. Tu and Ou-Yang (2002) summarized several different results presented by different authors and a large varying range of 0.5–5.5 TPa of Young's modulus was found. Several other experiments, theoretical models and MD simulations, were also carried out to predict the elastic properties of CNTs, and similar phenomena were also reported (Cagliero et al. 2015; Liew et al. 2004; Meo

and Rossi 2006; Treacy et al. 1996; Bao et al. 2004; Wong et al. 1997).

Following the available references, it can be easily found that the material properties of CNTs are affected by many factors, and it cannot be set as certain values. Under many circumstances, they should be considered as uncertain parameters with a range. To the authors' knowledge, the material parameters are sometimes treated as random variables in a few studies. For example, Scarpa and Adhikari (2008) established a stochastic reduced order model to analyze the natural frequencies of CNT terahertz oscillators. In their work, both the thickness and the mass density were defined as random variables, and the predictions calculated by the analytical models were also validated by comparing with FE models. Chang (2013a, b) proposed a stochastic finite element (FE) method to study the nonlinear vibration of the fluid-conveying double-walled CNTs. In his studies, the Young's modulus of the CNTs was characterized as random parameters. In fact, the influence of uncertain system parameters on the mechanical behaviors of fluid-conveying pipes has aroused widely concern in recent years. For instance, Ritto et al.(2014) studied the stochastic stability and reliability behaviors of the fluid-conveying pipe system by using a probabilistic model with consideration of the modeling errors. Gan et al.(2014) presented a random uncertainty modeling procedure to study the vibration characteristics of a straight pipe conveying fluid. Alizadeh et al.(2016) discussed the vibration and stability of fluid-conveying pipes by considering the structural and fluid parameters as random variables.

Probabilistic model can be used to describe the uncertain parameters. However, a large number of information should be offered to build a precise probability distribution function (PDF) for the uncertain parameters in the probabilistic model (Lv and Qiu 2016). Unfortunately, due to the small size effect, it is often too difficult to collect enough information about the uncertainty of nanostructures. To overcome the weaknesses of the probabilistic model, an interval analysis method is proposed in the present paper. In the interval model, the uncertain parameters can be defined as interval variables with deterministic bounds (Impollonia and Muscolino 2011). Because only the upper and lower bounds of the uncertain parameter are needed, the interval model can be effectively used to represent the uncertain parameters where the sample points are limited. As a matter of fact, the uncertain-but-bounded parameters are widely used in many engineering problems such as vibration, bulking, and static and dynamic characteristics of engineering structures (Impollonia and Muscolino 2011; Koyluoglu and Elishakoff 1998; Neumaier 1990; Rao and Berke 1997; Sofi and Muscolino 2015; Sofi et al. 2015a, b). However, an interval analysis model incorporating the

small-scale and uncertain-but-bounded parameters of CNTs has not been reported yet.

The wave dispersion behavior of CNTs has gained extensive attention from scientific communities because many crucial physical characteristics such as optical transition and electrical conductance and many dynamic behaviors of CNTs are directly related to the presence of waves. As far as the authors' awareness, many works have been reported on deterministic analysis of wave propagation characteristics of fluid-conveying CNTs, such as (Dong et al. 2007, 2008; Li and Hu 2016; Narendar and Gopalakrishnan 2010; Wang et al. 2013). However, no previous work is available in the literature to accomplish the wave propagation analysis of fluid-conveying CNTs with uncertain-but-bounded material and fluid properties. The main objective of this paper is to set up a theoretical model to investigate the influence of the uncertain-but-bounded parameters on wave propagation characteristics of fluid-conveying CNTs.

The paper is organized as follows. In the next section, a theoretical model is presented to characterize the wave propagation behavior of CNTs, and the small-scale effect is also taken into account by using the nonlocal elasticity theory. Besides, an iterative algorithm-based interval analysis method is proposed to account for the uncertain-but-bounded properties of the material and fluid. In Sect. 3, the presented interval analysis method is validated by comparing with the Monte Carlo simulation and the probabilistic model. In Sect. 4, the influence of the uncertain-but-bounded parameters of the material and fluid on wave dispersion behaviors of fluid-conveying CNTs is investigated in detail. Finally, conclusions are drawn in Sect. 5.

2 Problem formulation

2.1 Nonlocal continuum theory

Nonlocal continuum theory has been widely applied to CNTs because it can reflect the small-scale effect of CNTs. This theory assumes that the stress tensor at a reference points $\mathbf{x}$ is related to the whole strain field of the object under study. The nonlocal elasticity constitutive relation can be expressed in the differential form as (Eringen 1972)

$$\left(1 - (e_0 a)^2 \nabla^2\right)\boldsymbol{\sigma}(\mathbf{x}) = \mathbf{T}(\mathbf{x}), \quad \mathbf{T}(\mathbf{x}) = \mathbf{C}(\mathbf{x}) : \boldsymbol{\varepsilon}(\mathbf{x}), \quad (1)$$

where $\boldsymbol{\sigma}(\mathbf{x})$ and $\mathbf{T}(\mathbf{x})$ denote the nonlocal and local stress tensor components, respectively, and $\mathbf{C}(\mathbf{x})$ represents the fourth-order elasticity tensor, the symbol ":" denotes the "double-dot product," $\boldsymbol{\varepsilon}(\mathbf{x})$ denotes the strain tensor component, $e_0 a$ denotes the small-scale coefficient, and ∇^2 is the Laplacian operator. Note that the classical (local) elasticity theory can be recovered from $e_0 a = 0$.

In the special case of Euler–Bernoulli beams, Eq. (1) reduces to

$$\sigma_{xx} - (e_0 a)^2 \frac{\mathrm{d}^2 \sigma_{xx}}{\mathrm{d}x^2} = E\varepsilon_{xx} \tag{2}$$

where E represents Young's modulus of CNTs, σ_{xx} and ε_{xx} are axial stress and strain of CNTs, respectively.

2.2 Governing equations

To understand the wave propagation in fluid-conveying CNTs, a CNT with Young's modulus E, mass density ρ_c, outer radius R_o, inner radius R_i, and cross-sectional area A is considered. The conveying fluid is modeled as a steady flow of mass density ρ_f, and flowing with an axial uniform velocity V_f, as depicted in Fig. 1. Based on Euler–Bernoulli beam theory, the deformation fields of CNTs are denoted as

$$u(x,t) = -z\frac{\partial w}{\partial x} \tag{3}$$

$$w(x,t) = w(x,t). \tag{4}$$

According to the small deformation assumption, the only nonzero strain of the CNT is

$$\varepsilon_{xx} = \frac{\partial u}{\partial x} = -z\frac{\partial^2 w}{\partial x^2}. \tag{5}$$

The Euler–Bernoulli beam theory with considering the rotary inertia and nonlocal effects of the CNT is used to derive the governing equation of fluid-conveying CNTs, which have been presented by Li and Hu (2016). Neglecting the fluid viscosity and strain gradient effects in their study or based on the Hamilton's principle derived in "Appendix", the differential equation of motion of the fluid-conveying CNTs can be given by

$$\left(1 - (e_0 a)^2 \frac{\partial^2}{\partial x^2}\right)\left[\rho_c A \frac{\partial^2 w}{\partial t^2} - \rho_c I \frac{\partial^4 w}{\partial x^2 \partial t^2}\right.$$
$$\left. + m_f\left(\frac{\partial^2 w}{\partial t^2} + 2V_f \frac{\partial^2 w}{\partial x \partial t} + V_f^2 \frac{\partial^2 w}{\partial x^2}\right)\right] + EI\frac{\partial^4 w}{\partial x^4} = 0.$$
$$(6)$$

where m_f and I are, respectively, the mass per unit length of the fluid and the moment of inertia of the CNT, which can be determined by
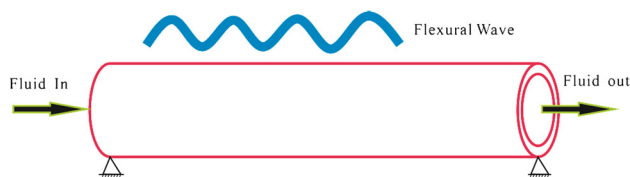

Fig. 1 Schematic of flexural wave propagation in a fluid-conveying CNT

$$m_f = \rho_f A_i, \quad I = \int_A z^2 \, dA, \tag{7}$$

where $A_i = \pi R_i^2$ denotes the inner internal cross-sectional area of the CNT.

In the wave propagation analysis, the transverse displacement of the fluid-conveying CNT is supposed to have the form as follows:

$$w = W \exp[-j(kx - \omega t)] \tag{8}$$

where W is the wave amplitude, k and ω are the wave number and the circular frequency, respectively, and $j = \sqrt{-1}$. Substituting Eqs. (8) into (6) leads to

$$\left(1 + (e_0 a)^2 k^2\right)\left[-\rho_c A \omega^2 - \rho_c I \omega^2 k^2 \right. \\ \left. - m_f\left(\omega^2 - 2V_f \omega k + V_f^2 k^2\right)\right] + EIk^4 = 0. \tag{9}$$

Then, the frequency can be calculated by

$$\omega = \frac{c_2 + \sqrt{c_2^2 + 4c_1 c_3}}{2c_1} \tag{10}$$

where the parameters c_1, c_2, and c_3 are, respectively, given as

$$c_1 = \left[1 + (e_0 a)^2 k^2\right]\left(\rho_c A + \rho_c I k^2 + m_f\right) \tag{11a}$$

$$c_2 = 2m_f V_f k \left[1 + (e_0 a)^2 k^2\right] \tag{11b}$$

$$c_3 = EIk^4 - \left[1 + (e_0 a)^2 k^2\right] m_f V_f^2 k^2. \tag{11c}$$

The phase velocity can be derived by using the following equation

$$c_p = \frac{\omega}{k}. \tag{12}$$

2.3 Interval analysis method

In the above section, the deterministic analysis for the wave propagation characteristics of fluid-conveying CNTs is presented. However, the system uncertainties caused by the manufacturing errors, physical imperfections, and material defects are unavoidable, and many experimental results have shown that the material properties of CNTs have a great of uncertainties. To overcome the massive information needed to build a precise PDF for the uncertain parameters to conduct the probabilistic analysis, the uncertain parameters are defined as interval variables with known bounds in this section. The material and fluid parameters, i.e., the mass density ρ_c, Young's modulus E of the CNT and the small-scale coefficient $e_0 a$, and the velocity V_f and mass density ρ_f of the conveying fluid, are

all defined as interval parameters. These uncertain parameters can be denoted by an interval vector as follows

$$\mathbf{z} \in \mathbf{z}^\mathbf{I} = [\underline{\mathbf{z}}, \overline{\mathbf{z}}] = [\mathbf{z}^\mathbf{c} - \Delta \mathbf{z}, \mathbf{z}^\mathbf{c} + \Delta \mathbf{z}] = \left(z_i^I\right), \tag{13a}$$

or $\quad z_i \in z_i^I = [\underline{z}_i, \overline{z}_i] = \left[z_i^c - \Delta z_i, z_i^c + \Delta z_i\right]$
$\quad i = 1, 2, \dots, 5$ \hfill (13b)

where $\underline{\mathbf{z}} = \left(\underline{z}_i\right)$ and $\overline{\mathbf{z}} = \left(\overline{z}_i\right)$ are, respectively, the lower and upper bounds of the uncertain parameter vector $\mathbf{z} = \left(E, \rho_c, e_0 a, V_f, \rho_f\right)^\mathrm{T}$; $\mathbf{z}^\mathbf{I} = \left(E^I, \rho_c^I, e_0 a^I, V_f^I, \rho_f^I\right)^\mathrm{T}$ is a five-dimensional interval vector including all uncertain material and fluid parameters; $z_i^c = \left(\underline{z}_i + \overline{z}_i\right)/2$ and $\Delta z_i = \left(\overline{z}_i - \underline{z}_i\right)/2$ represent the midpoint and the radius of the interval parameters, respectively. For simplicity, the radius of the uncertain-but-bounded parameter also can be represented by $\Delta z_i = \alpha z_i^c$, where the parameter α stands for the uncertain level. Accordingly, the interval parameter z_i^I can be denoted as $z_i^I = z_i^c [1 - \alpha, 1 + \alpha]$.

An interval analysis method based on the iterative algorithm is proposed to capture the lower and upper bounds of the wave dispersion curve. For the sake of generality, the interval extension of the wave dispersion relation expressed in Eq. (9) takes the form as follows:

$$F(\omega; \mathbf{z}^\mathbf{I}) = \left(1 + \left(e_0 a^I\right)^2 k^2\right)\left[-\rho_c^I A \omega^2 - \rho_c^I I \omega^2 k^2 \right. \\ \left. - \rho_f^I A_i\left(\omega^2 - 2V_f^I \omega k + \left(V_f^I k\right)^2\right)\right] + E^I I k^4 = 0 \tag{14}$$

where $F(\cdot)$ denotes a nonlinear function of the wave frequency ω, $F(\omega; \mathbf{z}^\mathbf{I})$ is the natural interval extension of $F(\omega; \mathbf{z})$.

The solution of Eq. (14) can be defined as a set

$$\Lambda = \omega(\mathbf{z}^\mathbf{I}) = \left\{\omega \in R : F(\omega; \mathbf{z}) = 0, \mathbf{z} \in \mathbf{z}^\mathbf{I}\right\} \tag{15}$$

where R denotes the real domain. One can notice that a direct solution to the above equation cannot be fulfilled due to the strong nonlinearity. Here, an iterative algorithm-based interval analysis method is proposed to solve the bounds of the wave frequency.

Firstly, we introduce two functions as follows

$$\phi(\omega) = \overline{F}(\omega; \mathbf{z}^\mathbf{I}) = \max_{\mathbf{z} \in \mathbf{z}^\mathbf{I}} F(\omega; \mathbf{z}) \tag{16}$$

$$\varphi(\omega) = \underline{F}(\omega; \mathbf{z}^\mathbf{I}) = \min_{\mathbf{z} \in \mathbf{z}^\mathbf{I}} F(\omega; \mathbf{z}) \tag{17}$$

where $\phi(\omega)$ and $\varphi(\omega)$ both can be treated as nonlinear functions of the wave frequency ω.

The first-order derivative of Eqs. (16) and (17) can be separately given as

$$\frac{d\phi(\omega)}{d\omega} = \frac{d}{d\omega}\left(\max_{\mathbf{z} \in \mathbf{z}^\mathbf{I}} F(\omega; \mathbf{z})\right) = \max_{\mathbf{z} \in \mathbf{z}^\mathbf{I}} \frac{\partial F(\omega; \mathbf{z})}{\partial \omega} \tag{18}$$

$$\frac{d\varphi(\omega)}{d\omega} = \frac{d}{d\omega}\left(\min_{\mathbf{z}\in\mathbf{z}^\mathbf{I}} F(\omega;\mathbf{z})\right) = \min_{\mathbf{z}\in\mathbf{z}^\mathbf{I}}\frac{\partial F(\omega;\mathbf{z})}{\partial\omega}. \tag{19}$$

Supposing $\omega = \omega_a$ as the solution of $\partial F(\omega;\mathbf{z})/\partial\omega = 0$, from Eq. (14), one has $\partial F(\omega;\mathbf{z}^\mathbf{I})/\partial\omega < 0$ when $\omega > \omega_a$, and then, it can be arrived at:

$$\begin{aligned}\frac{d\varphi(\omega)}{d\omega} &= \frac{d}{d\omega}\left(\min_{\mathbf{z}\in\mathbf{z}^\mathbf{I}} F(\omega;\mathbf{z})\right) < \frac{d\phi(\omega)}{d\omega} \\ &= \frac{d}{d\omega}\left(\max_{\mathbf{z}\in\mathbf{z}^\mathbf{I}} F(\omega;\mathbf{z})\right) < 0.\end{aligned} \tag{20}$$

Hence, it can be concluded that both $\phi(\omega)$ and $\varphi(\omega)$ are monotonically decreasing function with respect to the wave frequency ω when $\omega > \omega_a$.

Assuming that $\omega = \omega_*$ is the solution of equation $F(\omega;\mathbf{z}) = 0$ and by using monotonicity, one has

$$F(\omega_*;\mathbf{z}) \in F(\omega_*;\mathbf{z}^\mathbf{I}) \tag{21}$$

where $F(\omega_*;\mathbf{z}^\mathbf{I})$ is an interval extension of $F(\omega_*;\mathbf{z})$.

Combining $F(\omega_*;\mathbf{z}) = 0$ with Eqs. (16), (17), and (21), the following inequality can be derived as

$$\varphi(\omega_*) = \underline{F}(\omega_*;\mathbf{z}^\mathbf{I}) \leq 0 \leq \bar{F}(\omega_*;\mathbf{z}^\mathbf{I}) = \phi(\omega_*). \tag{22}$$
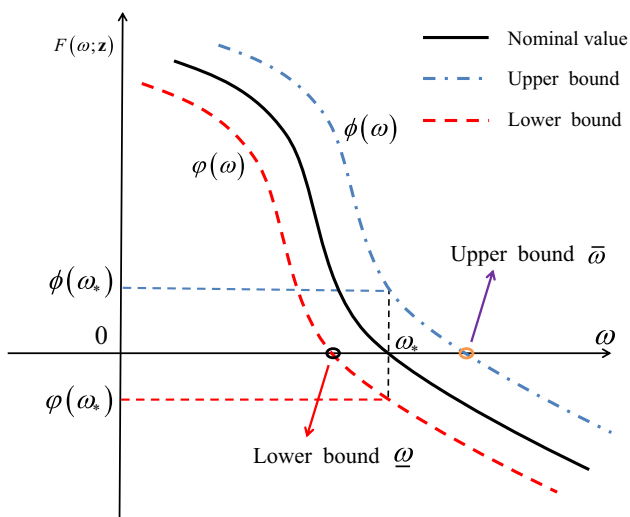
The above relationship is clearly found in Fig. 2. From this figure, the following two equations also can be obtained

$$\phi(\bar{\omega}) = \lim_{\omega_*\to\bar{\omega}}\phi(\omega_*) = 0 \tag{23}$$

$$\varphi(\underline{\omega}) = \lim_{\omega_*\to\underline{\omega}}\varphi(\omega_*) = 0 \tag{24}$$

where $\underline{\omega} = \min_{\mathbf{z}\in\mathbf{z}^\mathbf{I}}\omega(\mathbf{z})$ and $\bar{\omega} = \max_{\mathbf{z}\in\mathbf{z}^\mathbf{I}}\omega(\mathbf{z})$ are the lower and upper bounds of the wave frequency, respectively.

Introducing three interval vectors as follows

Fig. 2 Illustration of interval analysis method based on the iterative algorithm

$$\omega_S^I = [\underline{\omega}_S, \bar{\omega}_S], \quad \underline{\omega}_S \leq \underline{\omega} \leq \bar{\omega} \leq \bar{\omega}_S \tag{25}$$

$$\omega_U^I = [\underline{\omega}_U, \bar{\omega}_U], \quad \underline{\omega}_U \leq \bar{\omega} \leq \bar{\omega}_U \tag{26}$$

$$\omega_L^I = [\underline{\omega}_L, \bar{\omega}_L], \quad \underline{\omega}_L \leq \underline{\omega} \leq \bar{\omega}_L \tag{27}$$

where ω_S^I denotes an initial interval involving all possible values of the wave frequency set ω^I; ω_U^I and ω_L^I are iterative intervals of the upper and lower bounds of the wave frequency, respectively. $\underline{\omega}_b$ and $\bar{\omega}_b$ ($b = S$, U and L) denote the lower and upper bounds of the corresponding intervals, respectively.

In Eq. (23), the first-order Taylor series expansion at $\omega = \omega_*$ can be expressed as

$$\phi(\bar{\omega}) = \phi(\omega_*) + \frac{d\phi(\xi)}{d\omega}(\bar{\omega} - \omega_*) \tag{28}$$

where $\omega_* \leq \xi \leq \bar{\omega}$. By combining Eqs. (18), (25), and (26), and using monotonicity, and considering $\xi \in \omega_S^I$ and $\bar{\omega} \in \omega_U^I$, one has

$$\phi(\bar{\omega}) \in \phi(\omega_U^I) \subset \phi(\omega_*) + \frac{d\phi(\xi)}{d\omega}(\omega_U^I - \omega_*) \tag{29}$$

$$\frac{d\phi(\xi)}{d\omega} \in \frac{d\phi(\omega_S^I)}{d\omega} \subset \frac{\partial F(\omega_S^I;\mathbf{z}^\mathbf{I})}{\partial\omega} \tag{30}$$

where $d\phi(\omega_S^I)/d\omega$ and $\partial F(\omega_S^I;\mathbf{z}^\mathbf{I})/\partial\omega$ represent the interval extensions of $d\phi(\omega)/d\omega$ and $\partial F(\omega;\mathbf{z})/\partial\omega$, respectively.

Inserting Eqs. (23) and (30) into Eq. (29), the following equation can be obtained

$$0 \in \phi(\omega_*) + \frac{\partial F(\omega_S^I;\mathbf{z}^\mathbf{I})}{\partial\omega}(\omega_U^I - \omega_*). \tag{31}$$

Based on the interval mathematics, it is clear that the width of right-hand side interval given in Eq. (31) depends only on ω_U^I because the widths of both ω_S^I and $\mathbf{z}^\mathbf{I}$ are constants. Then there exists a constant λ_c satisfying (Alefeld and Mayer 2000; Moore 1979)

$$\text{Wid}\left(\phi(\omega_*) + \frac{\partial F(\omega_S^I;\mathbf{z}^\mathbf{I})}{\partial\omega}(\omega_U^I - \omega_*)\right) \leq \lambda_c\text{Wid}(\omega_U^I). \tag{32}$$

where $\text{Wid}(\cdot)$ represents the width of interval vector. Our goal is to obtain the upper bound of the wave frequency $\bar{\omega} \in \omega_U^I$ whose width is zero. Based on the interval analysis theory proposed by Moore (1979), if the interval arithmetic evaluation exists, then the width of ω_U^I is approaching zero. Correspondingly, the width of the interval arithmetic evaluation will go linearly to zero (Alefeld and Mayer 2000), i.e.,

$$\text{Wid}\left(\phi(\omega_*) + \frac{\partial F(\omega_S^I;\mathbf{z}^\mathbf{I})}{\partial\omega}(\omega_U^I - \omega_*)\right) \to 0. \tag{33}$$

Equation (33) provides an available method to identify the upper bound of frequency by an iterative algorithm to reduce the width of ω_U^I. The iterative algorithm can be established via the following equation

$$\phi(\omega_*) + \frac{\partial F(\omega_S^I; \mathbf{z^I})}{\partial \omega}(\omega_U^I - \omega_*) = 0. \tag{34}$$

Because $\phi(\omega_*) \geq 0$ and $\partial F(\omega_S^I; \mathbf{z^I})/\partial \omega < 0$, the iterative interval ω_U^I can be obtained by Eq. (34), which can be further expressed as

$$\omega_U^I = [\underline{\omega}_U, \bar{\omega}_U] = \left[\omega_* - \frac{\phi(\omega_*)}{\underline{d}}, \; \omega_* - \frac{\phi(\omega_*)}{\bar{d}}\right] \tag{35}$$

where

$$\underline{d} = \min_{\omega \in \omega_S^I, \mathbf{z} \in \mathbf{z^I}} \frac{\partial F(\omega; \mathbf{z})}{\partial \omega}, \quad \bar{d} = \max_{\omega \in \omega_S^I, \mathbf{z} \in \mathbf{z^I}} \frac{\partial F(\omega; \mathbf{z})}{\partial \omega}. \tag{36}$$

Substituting $\bar{\omega} \in \omega_U^I$ into Eq. (35) leads to

$$\omega_* - \frac{\phi(\omega_*)}{\underline{d}} \leq \bar{\omega} \leq \omega_* - \frac{\phi(\omega_*)}{\bar{d}}. \tag{37}$$

Because $\phi(\omega_*)/\underline{d} \leq 0$, one can also have

$$\omega_* \leq \omega_* - \frac{\phi(\omega_*)}{\underline{d}} \leq \bar{\omega}. \tag{38}$$

Based on the above inequality, the iterative algorithm for the upper bound of the wave frequency can be determined by

$$\bar{\omega}_{p+1} = \bar{\omega}_p - \frac{\phi(\bar{\omega}_p)}{\underline{d}} \tag{39}$$

where $\bar{\omega}_p$ is the iterative wave frequency of the pth computational cycle during the iterative procedure. The convergent condition is given as follows

$$|\bar{\omega}_{p+1} - \bar{\omega}_p| \leq \theta. \tag{40}$$

The upper bound of the wave frequency can be determined at the point when the above convergent condition is satisfied. The algorithm flowchart for the interval analysis is shown in Fig. 3.

Similarly, following the steps presented in Eqs. (28)–(39), the iterative algorithm for the lower bound of the wave frequency also can be calculated by

$$\underline{\omega}_{q+1} = \underline{\omega}_q - \frac{\varphi(\underline{\omega}_q)}{\underline{d}} \tag{41}$$

where $\underline{\omega}_q$ denotes the iterative frequency of the qth computational cycle during the iterative procedure. Combining with the convergent condition, the lower bound of the wave frequency can be obtained. The bounds of the phase velocity also can be calculated in the same way.
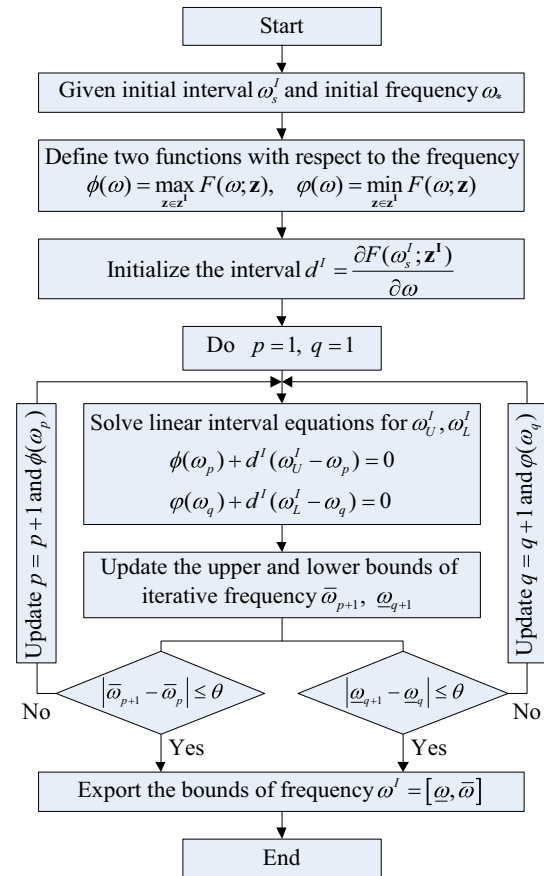

Fig. 3 Algorithm flowchart for the interval analysis of wave propagation in fluid-conveying CNTs

2.4 Probabilistic analysis method

In this section, a probabilistic model is presented to validate the interval analysis method proposed in the above section. Assume that the uncertain material and fluid parameter vector $\mathbf{z} = (E, \rho_c, e_0 a, V_f, \rho_f)^{\mathrm{T}}$ is random variable. Denote the wave frequency expressed in Eq. (10) as a function $\omega(\mathbf{z})$. Then, the wave frequency $\omega(\mathbf{z})$ is also random. The mean value of the random parameter vector $\mathbf{z}$ can be given as

$$E(\mathbf{z}) = (E(z_i)) = \mathbf{z}^E = (z_i^E). \tag{42}$$

Using first-order Taylor series expansion, the wave frequency $\omega(\mathbf{z})$ about the mean value $\mathbf{z}^E$ is developed as

$$\omega(\mathbf{z}) = \omega(\mathbf{z}^E + \delta) = \omega(\mathbf{z}^E) + \sum_{i=1}^n \frac{\partial \omega(\mathbf{z}^E)}{\partial z_i}(z_i - z_i^E). \tag{43}$$

The mean value of the wave frequency can be obtained by taking the expected value of both sides of Eq. (43). One can arrive at

$$E(\omega(\mathbf{z})) = E\big(\omega(\mathbf{z}^E)\big) + E\left(\sum_{i=1}^{n}\frac{\partial\omega(\mathbf{z}^E)}{\partial z_i}(z_i - z_i^E)\right)$$
$$= \omega(\mathbf{z}^E) + \sum_{i=1}^{n}\frac{\partial\omega(\mathbf{z}^E)}{\partial z_i}E(z_i - z_i^E) \qquad (44)$$

It is noted that $E(z_i - z_i^E)$ is zero, and thus, one has

$$E(\omega(\mathbf{z})) = \omega(\mathbf{z}^E). \qquad (45)$$

In a similar way, the variance of the wave frequency can be calculated as follows:

$$D(\omega(\mathbf{z})) = \sum_{i=1}^{n}\left(\frac{\partial\omega(\mathbf{z}^E)}{\partial z_i}\right)^2 D(z_i)$$
$$+ \sum_{i=1}^{n}\sum_{l=1}^{n}\frac{\partial\omega(\mathbf{z}^E)}{\partial z_i}\frac{\partial\omega(\mathbf{z}^E)}{\partial z_l}\mathrm{Cov}(z_i, z_l). \qquad (46)$$

where $\mathrm{Cov}(z_i, z_l)$ is the covariance of the random parameter variables. When the random parameters are independent, one has $\mathrm{Cov}(z_i, z_l) = 0$, and then Eq. (46) is reduced as

$$D(\omega(\mathbf{z})) = \sum_{i=1}^{n}\left(\frac{\partial\omega(\mathbf{z}^E)}{\partial z_i}\right)^2 D(z_i) = \sum_{i=1}^{n}\left(\frac{\partial\omega(\mathbf{z}^E)}{\partial z_i}\sigma(z_i)\right)^2$$
$$= \sum_{i=1}^{n}\left(\frac{\partial\omega(\mathbf{z}^E)}{\partial z_i}\sigma_i\right)^2 \qquad (47)$$

where $\sigma(\mathbf{z}) = (\sigma(z_i))$ is the standard deviation of the random parameter vector $\mathbf{z} = (z_i)$, and then, the standard deviation of the wave frequency can be derived as

$$\sigma(\omega(\mathbf{z})) = \sqrt{D(\omega(\mathbf{z}))} = \sqrt{\sum_{i=1}^{n}\left(\frac{\partial\omega(\mathbf{z}^E)}{\partial z_i}\sigma_i\right)^2}. \qquad (48)$$

The probabilistic range of g times standard deviations of the mean value of the wave frequency can be denoted as

$$\omega^I = [\underline{\omega}(\mathbf{z}), \bar{\omega}(\mathbf{z})]$$
$$= \big[\omega(\mathbf{z}^E) - g\sigma(\omega(\mathbf{z})), \omega(\mathbf{z}^E) + g\sigma(\omega(\mathbf{z}))\big] \qquad (49)$$

where $\underline{\omega}(\mathbf{z})$ and $\bar{\omega}(\mathbf{z})$ are, respectively, the probabilistic lower and upper bounds of the wave frequency obtained by the probabilistic method; g is a positive integer and can be determined by the intervals of the uncertain-but-bounded parameters. Similarly, the probabilistic lower and upper bounds of the phase velocity also can be obtained.

3 Model verification

In this section, the Monte Carlo simulation and the probabilistic model are employed to verify the present interval analysis method. The inner and outer radiuses of the CNT are defined as $R_i = 3.4$ nm and $R_o = 3.74$ nm, respectively (Zhen et al. 2011). The material parameters

(including the Young's modulus E, mass density ρ_c, and the small-scale coefficient e_0a of the CNTs) and the fluid parameters (including the velocity V_f and the mass density ρ_f of the fluid) are all treated as uncertain-but-bounded parameters. The midpoints of these interval parameters are, respectively, defined as (Zhen et al. 2011) $E^c = 1$ TPa, $\rho_c^c = 2300$ kg/m^3, $e_0a^c = 0.5$ nm, $V_f^c = 1000$ m/s, and $\rho_f^c = 1000$ kg/m^3, while the radiuses of these parameters are expressed as $\Delta E = \alpha E^c$, $\Delta\rho_c = \alpha\rho_c^c$, $\Delta e_0a = \alpha \cdot e_0a^c$, $\Delta V_f = \alpha V_f^c$ and $\Delta\rho_f = \alpha\rho_f^c$, respectively, where the variable α represents the uncertainty level.

## 3.1 Comparison with Monte Carlo simulation

The lower bound (LB) and upper bound (UB) of the wave dispersion curves calculated by the present interval analysis method (IAM) and Monte Carlo simulation (MCS) are compared and shown in Fig. 4. Here, the MCS with 3.2×10^6 sample points is introduced as a referenced method, and it can be performed in the following steps. Firstly, we choose 20 equal incremental values for each uncertain parameter from its LB to UB. Then a large number of deterministic wave frequency and phase velocity responses can be obtained by using Eqs. (10) and (12), from which the maximum and minimum of the wave dispersion curves with respect to the interval parameters can be easily obtained. As depicted in Fig. 4, the UB of the wave frequency and the phase velocity predicted by the IAM is a little lower than that predicted by the MCS, while the LB of the frequency and the phase velocity obtained by the IAM is a little larger than that obtained by the MCS. In other words, the wave dispersion curves predicted by the present IAM is completely reliable and can extensively reduce the computational cost for huge samples of MCS.

3.2 Comparison with probabilistic analysis method

The probabilistic analysis method (PAM) is presented to validate the IAM. We assume that the Young's modulus E, mass density ρ_c, and the small-scale coefficient e_0a of the CNTs, and the velocity V_f and mass density ρ_f of the fluid all have normal distributions with the mean values $\mu_E = 1$ TPa, $\mu_{\rho_c} = 2300$ kg/m^3, $\mu_{e_0a} = 0.5$ nm, $\mu_{V_f} = 1000$ m/s and $\mu_{\rho_f} = 1000$ kg/m^3, respectively. Based on 3σ principle, the standard deviations of these uncertain variables are set as $\sigma_E = 0.03$ TPa, $\sigma_{\rho_c} = 69$ kg/m^3, $\sigma_{e_0a} = 0.015$ nm, $\sigma_{V_f} = 30$ m/s and $\sigma_{\rho_f} = 30$ kg/m^3, respectively, which corresponds to the uncertain-but-bounded parameters with uncertainty level $\alpha = 0.09$. The comparison between IAM and PAM for the wave dispersion curves is depicted in Fig. 5. It is clear that the ranges of the wave frequency and phase velocity yielded by IAM
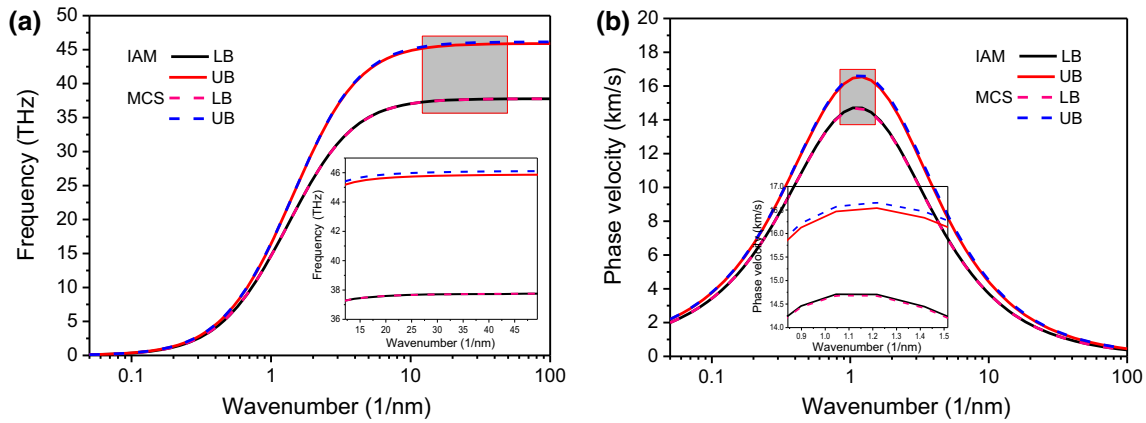
Fig. 4 Bounds of dispersion curves predicted by IAM and MCS: **a** wave frequency, **b** phase velocity. Here, the uncertainty level $\alpha = 0.05$ and the midpoint of the small-scale coefficient $e_0 a^c = 0.5$ nm are adopted
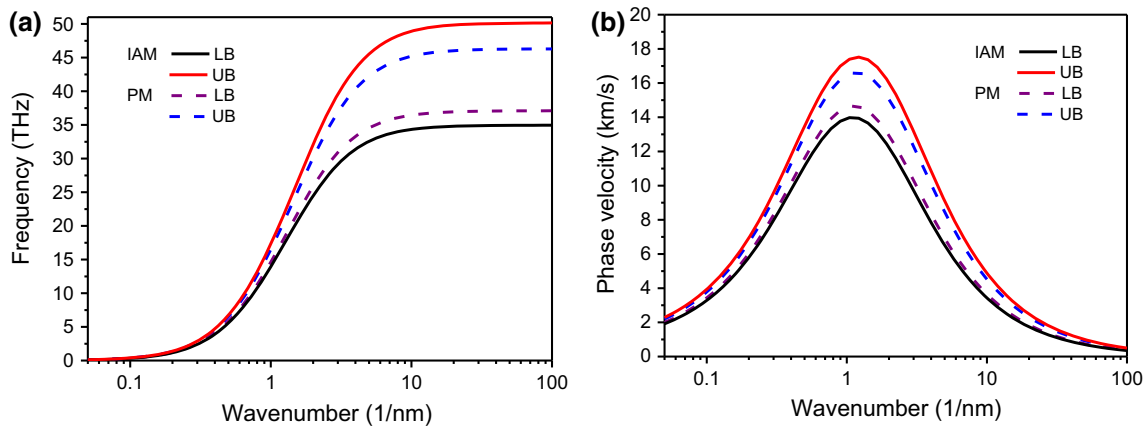
Fig. 5 Bounds of dispersion curves predicted by IAM with uncertainty level $\alpha = 0.09$ and PAM based on 3σ principle: **a** wave frequency, **b** phase velocity. Here, the midpoint of the small-scale coefficient $e_0 a^c = 0.5$ nm is adopted

are basically in well agreement with those predicted by PAM, but the former encloses the latter, which means the present IAM provides more conservative results than PAM.

4 Results and discussion

4.1 Parameter sensitivity studies

To identify the most important uncertain parameters which have the highest contributions to the wave propagation behaviors of fluid-conveying CNTs, the parameter sensitivity study is carried out in this section. The sensitivities of the wave frequency to uncertainty can be studied by using the relative sensitivity indices $S(z_i)$ defined as follows (Isukapalli 1999)

$$S(z_i) = \left| \frac{\partial \omega(\mathbf{z})}{\partial z_i} \right| \frac{|z_i^c|}{\omega_c(\mathbf{z})} \tag{50}$$

where $\omega_c(\mathbf{z})$ denotes the normal value of the wave frequency. The sensitivities of the wave frequency with

respect to the uncertain variables at several different wave numbers are compared in Table 1. It is observed that $S(E)$, $S(\rho_c)$, and $S(e_0 a)$ monotonically increase, and $S(\rho_f)$ and $S(V_f)$ monotonically decrease with increasing the wave number. The wave frequency is more sensitive to the small-scale coefficient $e_0 a$ than other uncertain parameters. At small wave numbers, the contribution of the small-scale coefficient $e_0 a$ is the lowest, while it shows the largest contribution to the wave frequency when the wave number becomes large. The Young's modulus E has the largest influence on the wave frequency when the wave number is small, while for larger wave numbers, the sensitivity of the mass density of the fluid is the lowest.
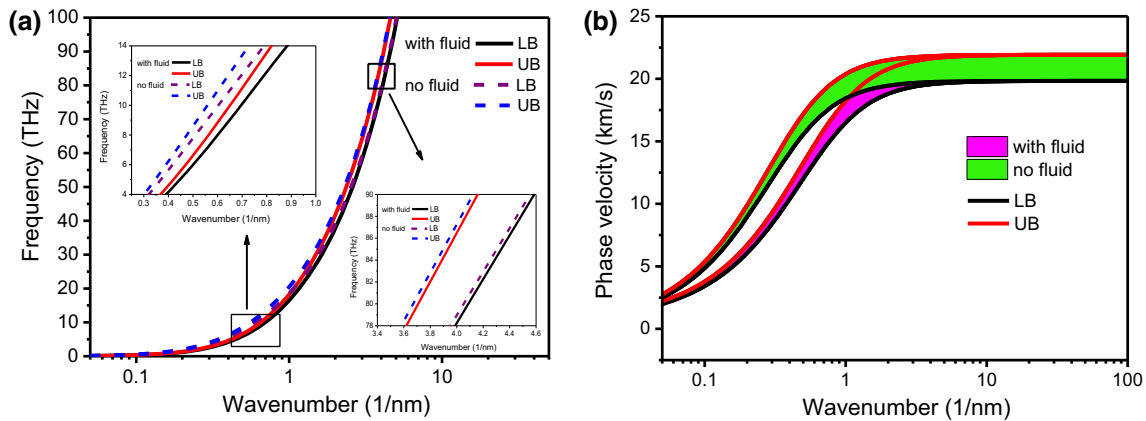
4.2 Effect of conveying fluid

The influences of the conveying fluid on the upper and lower bounds of the wave dispersion behaviors for the classical and nonlocal continuum models are depicted in Figs. 6 and 7, respectively. One can find that the conveying

Table 1 Relative sensitivity of wave frequency with respect to uncertain variables at different wave numbers

Sensitivity	$S(E)$	$S(\rho_c)$	$S(e_0a)$	$S(V_f)$	$S(\rho_f)$
$k = 0.1$ nm^{-1}	0.4188	0.2079	2.088×10^{-3}	0.1625	0.2108
$k = 1$ nm^{-1}	0.4933	0.3961	0.1973	0.0134	0.0972
$k = 10$ nm^{-1}	0.4997	0.4988	0.9610	5.972×10^{-4}	9.203×10^{-4}
$k = 100$ nm^{-1}	0.5000	0.5000	0.9997	1.087×10^{-4}	3.170×10^{-5}

Fig. 6 Bounds of dispersion curves for CNTs with or without conveying fluid predicted by the classical continuum model: **a** wave frequency, **b** phase velocity. Here, the uncertainty level $\alpha = 0.05$ and the small-scale coefficient $e_0a = 0$ nm are adopted

fluid will primarily affect the bounds of the wave frequency and phase velocity at small wave numbers both for the classical and nonlocal continuum models, while the bounds of the frequency and phase velocity are insignificant to the conveying fluid as the wave number is getting larger.

As depicted in Fig. 6a, the upper and lower bounds of the frequency always increase with increasing the wave number when the nonlocal effect is ignored. While from Fig. 7a, the bounds of the frequency increase firstly and then trend to constant values with increasing the wave number once the nonlocal effect is taken into account. Figure 7b gives the phase velocity versus the wave number with considering the small size effect, which shows that the conveying fluid will reduce both the upper and lower bounds of the phase velocity when $k < 3$ nm^{-1}, while the influence of the conveying fluid on the phase velocity dispersion curve is not much prominent when $k > 3$ nm^{-1}. The phase velocity has the widest range when the wave number k approaches to 1 nm^{-1}. However, as shown in Fig. 6b, when the small size effect is ignored, the range of the phase velocity will trend to constant values as $k > 4$ nm^{-1}. The significant deviation shown in Figs. 6 and 7 demonstrates that the small size scale has much effect on the bounds of the wave frequency and phase velocity, and its effect should not be neglected for the wave propagation analysis of the size-dependent fluid-conveying CNTs.

4.3 Effect of size-scale parameter

The bounds of the frequency dispersion curve for CNTs with several different size scales are illustrated in Fig. 8a. Here, $e_0a = 0$ nm represents the classical continuum model with no size-scale effect, $e_0a^c = 0.5$ nm, 1.0 and 2.0 nm denote three different midpoints of the small-scale coefficient. It is clear that the frequency increases dramatically all along the wave number as $e_0a = 0$ nm, while the wave frequency increases firstly and then tends to constant values when the size-scale effect is taken into account. The extensive deviation indicates the classical continuum model cannot be used to reflect the physical behavior of nanoscale CNTs. It is also shown that for a fixed e_0a^c, the range of the frequency increases firstly and then remains unchanged with respect to the wave number. As the parameters e_0a^c increases, the range of the frequency will become much narrower.

Figure 8b plots the upper and lower bounds of phase velocity dispersion curves for CNTs with uncertain variables at different size scales. The phase velocity is not sensitive to the midpoint of the small-scale coefficient e_0a^c when the wavelength is large (low wave numbers). However, once the wavelength is small (large wave numbers), the parameter e_0a^c will become important. The range of the phase velocity always increases with the wave number as the wavelength is large. However, if the wavelength is small, the bound of the phase velocity will remain
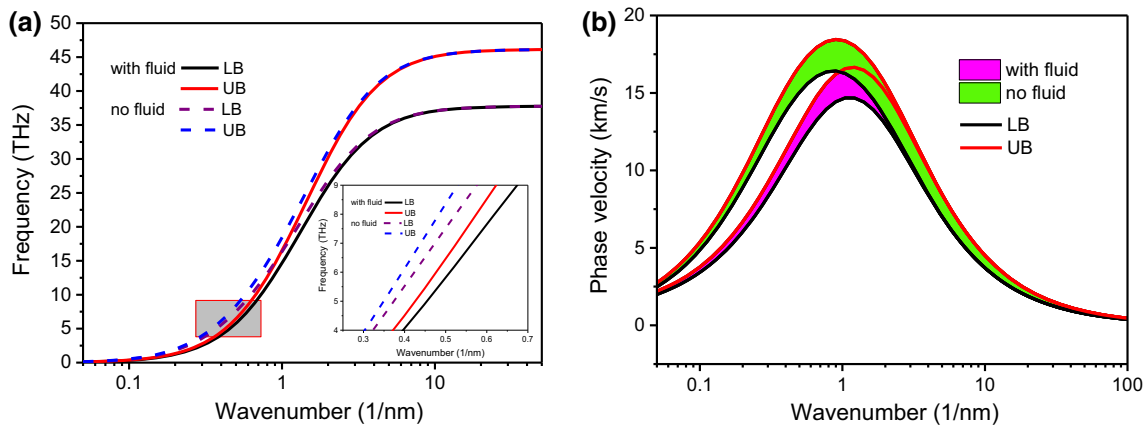
Fig. 7 Bounds of dispersion curves for CNTs with or without conveying fluid predicted by the nonlocal continuum model: **a** wave frequency, **b** phase velocity. Here, the uncertainty level $\alpha = 0.05$ and the midpoint of the small-scale coefficient $e_0 a^c = 0.5$ nm are adopted
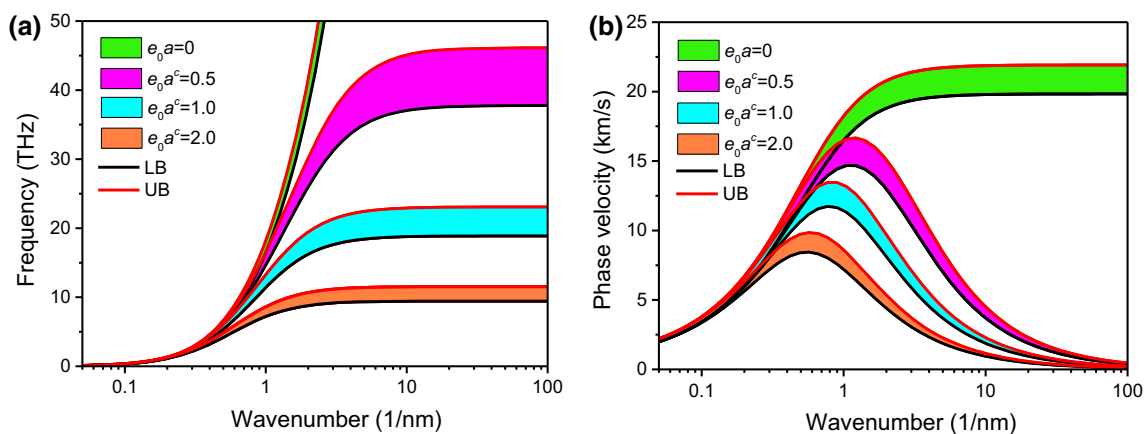
Fig. 8 Bounds of dispersion curves for CNTs with different size scales: **a** wave frequency, **b** phase velocity. Here, the uncertainty level is defined as $\alpha = 0.05$

unchanged when the size-dependent effect is ignored ($e_0 a = 0$ nm), while it decreases dramatically when the size-scale effect is taken into consideration. The observed deviation also confirms that the size-scale effect should not be neglected in analysis of CNTs conveying fluids.

4.4 Effect of uncertainty level

The uncertainty level which governs the uncertain-but-bounded variables is discussed in this section. The bounds of the wave frequency and the phase velocity as a function of the uncertain level are presented in Fig. 9. For the classical continuum model, the small-scale coefficient is defined as $e_0 a = 0$ nm, while the midpoint of small-scale coefficient $e_0 a^c = 0.5$ nm is used for the nonlocal continuum model. It is evident that the UB of the wave frequency and the phase velocity increases with increasing the uncertainty level both for the classical and nonlocal continuum models, while the LB of these characteristic variables shows an opposite tendency. Due to this fact, the

range of the wave frequency and the phase velocity will become larger as the uncertainty level increases. Compared with the classical continuum model, the upper and lower bounds of the wave frequency and the phase velocity both will reduce significantly when the size-scale effect is taken into consideration, which indicates the size-scale effect should not be neglected to analyze the wave propagation behaviors of fluid-conveying CNTs.

5 Conclusion

In this paper, an iterative algorithm-based interval analysis method is proposed to study the flexural wave propagation characteristics of fluid-conveying CNTs with system uncertainties. To deal with the uncertainties where few data are available to establish a precise PDF for probabilistic analysis, both the material properties of CNTs and the properties of the conveying fluid are all set as uncertain-but-bounded parameters. The governing equations are
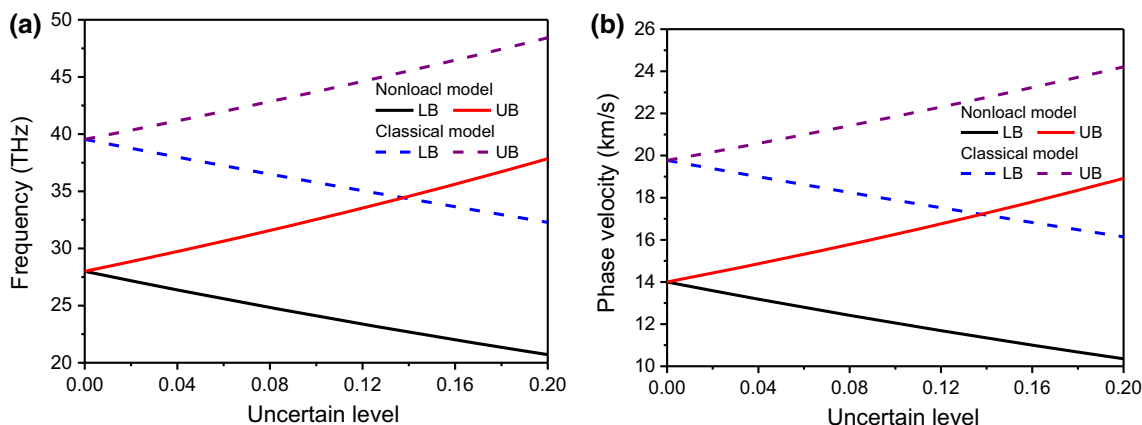
Fig. 9 Bounds of wave frequency and phase velocity at varying uncertain levels for classical and nonlocal continuum models. Here, the wave number is fixed as $k = 2 \text{ nm}^{-1}$

derived on the basis of nonlocal Euler–Bernoulli beam theory. Moreover, the upper and lower bounds of the wave dispersion curves are captured by using the proposed interval analysis method.

It can be concluded that both the fluid and the size-scale parameter will affect the upper and upper bounds of the wave frequency and phase velocity significantly. The uncertain level also has considerable influences on the upper and upper bounds of the wave frequency and the phase velocity. The proposed method is also verified by comparing with the Monte Carlo method and probabilistic method, and good agreements are achieved. Comparing with these two traditional uncertain analysis methods, the proposed interval method can reduce the large computational cost of Monte Carlo simulations and can overcome the large prior information needed in probabilistic analyses. The presented interval analysis method presents one useful way to investigate the uncertain effect in small-scale CNTs and also can be used in other nanostructures with uncertain system properties.

Appendix

The Hamilton's principle is used to obtain the governing equations of CNTs, which reads

$$\int_{t_1}^{t_2} \delta\left(U - T_f - T_c\right) \mathrm{d}t = 0 \tag{51}$$

where U, T_f, and T_c denote potential energy, kinetic energy of fluid and CNT, respectively.

The first variation of potential energy of the CNT can be expressed as

$$
\begin{aligned}
\delta U &= \int_V \sigma_{xx}\delta\varepsilon_{xx}\mathrm{d}V = -\int_V \sigma_{xx}\delta\left(z\frac{\partial^2 w}{\partial x^2}\right)\mathrm{d}V \\
&= -\int_0^L \frac{\partial^2 M}{\partial x^2}\delta w\,\mathrm{d}x
\end{aligned} \tag{52}
$$

where M represents the bending moment, which satisfies

$$M = \int_A z\sigma_{xx}\mathrm{d}A. \tag{53}$$

The first variation of the kinetic energy of the CNT and the conveying fluid can be separately expressed as

$$
\begin{aligned}
\delta T_c &= \int_0^L \int_A \left[\rho_c\left(\frac{\partial w}{\partial t}\delta\left(\frac{\partial w}{\partial t}\right) + \left(z\frac{\partial^2 w}{\partial t\partial x}\right)\delta\left(z\frac{\partial^2 w}{\partial t\partial x}\right)\right)\right]\mathrm{d}A\mathrm{d}x \\
&= \int_0^L \left(-\rho_c A\frac{\partial^2 w}{\partial t^2} + \rho_c I\frac{\partial^4 w}{\partial t^2\partial x^2}\right)\delta w\,\mathrm{d}x
\end{aligned} \tag{54}
$$

$$
\begin{aligned}
\delta T_f &= m_f \int_0^L \left(\frac{\partial w}{\partial t}\delta\left(\frac{\partial w}{\partial t}\right) + V_f\delta\left(\frac{\partial w}{\partial t}\frac{\partial w}{\partial x}\right) + V_f^2\frac{\partial w}{\partial x}\delta\left(\frac{\partial w}{\partial x}\right)\right)\mathrm{d}x \\
&= -m_f \int_0^L \left(\frac{\partial^2 w}{\partial t^2} + 2V_f\frac{\partial^2 w}{\partial t\partial x} + V_f^2\frac{\partial^2 w}{\partial x^2}\right)\delta w\,\mathrm{d}x
\end{aligned} \tag{55}
$$

where $m_f = \rho_f \times A_i$ is the mass of fluid per unit length, I is the moment of inertia of the CNT, which can be determined by

$$I = \int_A z^2\mathrm{d}A. \tag{56}$$

Substituting Eqs. (52), (54), and (55) into Eq. (51), and setting the coefficient of δw to zero, the governing equations of motion can be obtained as

$$
\begin{aligned}
\frac{\partial^2 M}{\partial x^2} &= \rho_c A\frac{\partial^2 w}{\partial t^2} - \rho_c I\frac{\partial^4 w}{\partial x^2\partial t^2} \\
&\quad + m_f\left(\frac{\partial^2 w}{\partial t^2} + 2V_f\frac{\partial^2 w}{\partial x\partial t} + V_f^2\frac{\partial^2 w}{\partial x^2}\right).
\end{aligned} \tag{57}
$$

Multiplying Eq. (2) by z and integrating the corresponding equation over the cross-sectional area A leads to

$$M - (e_0 a)^2 \frac{\partial^2 M}{\partial x^2} = E \int_A \left(-z^2 w_{,xx}\right) \mathrm{d}A = -EI \frac{\partial^2 w}{\partial x^2}. \qquad (58)$$

By introducing Eqs. (57) to (58), the bending moment can be given as

$$\begin{aligned} M = (e_0 a)^2 &\left[\rho_c A \frac{\partial^2 w}{\partial t^2} - \rho_c I \frac{\partial^4 w}{\partial x^2 \partial t^2} \right.\\ &\left. + m_f \left(\frac{\partial^2 w}{\partial t^2} + 2V_f \frac{\partial^2 w}{\partial x \partial t} + V_f^2 \frac{\partial^2 w}{\partial x^2} \right) \right] - EI \frac{\partial^2 w}{\partial x^2}. \end{aligned} \qquad (59)$$

Substituting Eqs. (59) into (57), the differential equation of motion of fluid-conveying CNTs can be expressed as

$$\begin{aligned} \left(1 - (e_0 a)^2 \frac{\partial^2}{\partial x^2} \right) &\left[\rho_c A \frac{\partial^2 w}{\partial t^2} - \rho_c I \frac{\partial^4 w}{\partial x^2 \partial t^2} \right.\\ &\left. + m_f \left(\frac{\partial^2 w}{\partial t^2} + 2V_f \frac{\partial^2 w}{\partial x \partial t} + V_f^2 \frac{\partial^2 w}{\partial x^2} \right) \right] + EI \frac{\partial^4 w}{\partial x^4} = 0. \end{aligned} \qquad (60)$$

References

Abbasnejad B, Shabani R, Rezazadeh G (2015) Stability analysis of a piezoelectrically actuated micro-pipe conveying fluid. Microfluid Nanofluid 19(3):577–584

Adali S (2008) Variational principles for multi-walled carbon nanotubes undergoing buckling based on nonlocal elasticity theory. Phys Lett A 372(35):5701–5705

Alefeld G, Mayer G (2000) Interval analysis: theory and applications. J Comput Appl Math 121:421–464

Alizadeh AA, Mirdamadi HR, Pishevar A (2016) Reliability analysis of pipe conveying fluid with stochastic structural and fluid parameters. Eng Struct 122:24–32

Amara K, Tounsi A, Mechab I, Adda-Bedia EA (2010) Nonlocal elasticity effect on column buckling of multiwalled carbon nanotubes under temperature field. Appl Math Model 34(12):3933–3942

Amiri A, Pournaki IJ, Jafarzadeh E, Shabani R, Rezazadeh G (2016) Vibration and instability of fluid-conveyed smart micro-tubes based on magneto-electro-elasticity beam model. Microfluid Nanofluid 20(2):1–10

Ansari R, Gholami R, Norouzzadeh A, Sahmani S (2015) Size-dependent vibration and instability of fluid-conveying functionally graded microshells based on the modified couple stress theory. Microfluid Nanofluid 19(3):509–522

Ansari R, Norouzzadeh A, Gholami R, Faghih Shojaei M, Darabi MA (2016) Geometrically nonlinear free vibration and instability of fluid-conveying nanoscale pipes including surface stress effects. Microfluid Nanofluid 20(1):28

Aydogdu M (2014) Longitudinal wave propagation in multiwalled carbon nanotubes. Compos Struct 107:578–584

Bahaadini R, Hosseini M (2016) Nonlocal divergence and flutter instability analysis of embedded fluid-conveying carbon nanotube under magnetic field. Microfluid Nanofluid 20(7):1–14

Bao WX, Zhu CC, Cui WZ (2004) Simulation of Young's modulus of single-walled carbon nanotubes by molecular dynamics. Phys B 352(1):156–163

Cagliero R, Barbato G, Maizza G, Genta G (2015) Measurement of elastic modulus by instrumented indentation in the macro-range: uncertainty evaluation. Int J Mech Sci 101–102:161–169

Chang TP (2013a) Nonlinear thermal-mechanical vibration of flow-conveying double-walled carbon nanotubes subjected to random material property. Microfluid Nanofluid 15(2):219–229

Chang TP (2013b) Stochastic FEM on nonlinear vibration of fluid-loaded double-walled carbon nanotubes subjected to a moving load based on nonlocal elasticity theory. Compos Part B Eng 54:391–399

De Rosa MA, Lippiello M (2017) Nonlocal Timoshenko frequency analysis of single-walled carbon nanotube with attached mass: an alternative hamiltonian approach. Compos Part B Eng 111:409–418

Deng Q, Yang Z (2014) Vibration of fluid-filled multi-walled carbon nanotubes seen via nonlocal elasticity theory. Acta Mech Solida Sin 27(6):568–578

Dong K, Wang X, Sheng GG (2007) Wave dispersion characteristics in fluid-filled carbon nanotubes embedded in an elastic medium. Model Simul Mater Sci Eng 15(5):427–439

Dong K, Liu BY, Wang X (2008) Wave propagation in fluid-filled multi-walled carbon nanotubes embedded in elastic matrix. Comput Mater Sci 42(1):139–148

Ebrahimi F, Nasirzadeh P (2015) Small-scale effects on transverse vibrational behavior of single-walled carbon nanotubes with arbitrary boundary conditions. Eng Solid Mech 3(2):131–141

Eringen AC (1972) Nonlocal polar elastic continua. Int J Eng Sci 10(1):1–16

Gan CB, Guo SQ, Lei H, Yang SX (2014) Random uncertainty modeling and vibration analysis of a straight pipe conveying fluid. Nonlinear Dyn 77:503–519

Hanasaki I, Nakatani A (2006) Water flow through carbon nanotube junctions as molecular convergent nozzles. Nanotechnology 17(11):2794–2804

Hu YG, Liew KM, Wang Q (2012) Modeling of vibrations of carbon nanotubes. Procedia Eng 31:343–347

Huang Y, Luo QZ, Li XF (2013) Transverse waves propagating in carbon nanotubes via a higher-order nonlocal beam model. Compos Struct 95:328–336

Iijima S (1991) Helical microtubes of graphite carbon. Nature 354:56–58

Impollonia N, Muscolino G (2011) Interval analysis of structures with uncertain-but-bounded axial stiffness. Comput Meth Appl Mech Eng 200(21):1945–1962

Isukapalli SS (1999) Uncertainty analysis of transport-transformation models. Doctoral dissertation, Rutgers, The State University of New Jersey

Khademolhosseini F, Rajapakse RKND, Nojeh A (2010) Torsional buckling of carbon nanotubes based on nonlocal elasticity shell models. Comput Mater Sci 48(4):736–742

Kiani K (2013a) Longitudinal, transverse, and torsional vibrations and stabilities of axially moving single-walled carbon nanotubes. Curr Appl Phys 13(8):1651–1660

Kiani K (2013b) Vibration behavior of simply supported inclined single-walled carbon nanotubes conveying viscous fluids flow using nonlocal Rayleigh beam model. Appl Math Model 37(4):1836–1850

Koyluoglu HU, Elishakoff I (1998) A comparison of stochastic and interval finite elements applied to shear frames with uncertain stiffness properties. Comput Struct 67(1):91–98

Krishnan A, Dujardin E, Ebbesen TW, Yianilos PN, Treacy MMJ (1998) Young's modulus of single-walled nanotubes. Phys Rev B 58(20):14013–14019

Li L, Hu Y (2016) Wave propagation in fluid-conveying viscoelastic carbon nanotubes based on nonlocal strain gradient theory. Comput Mater Sci 112:282–288

Li L, Hu Y, Li X, Ling L (2016) Size-dependent effects on critical flow velocity of fluid-conveying microtubes via nonlocal strain gradient theory. Microfluid Nanofluid 20(5):1–12

Liew KM, He XQ, Wong CH (2004) On the study of elastic and plastic properties of multi-walled carbon nanotubes under axial tension using molecular dynamics simulation. Acta Mater 52(9):2521–2527

Lv Z, Qiu Z (2016) A direct probabilistic approach to solve state equations for nonlinear systems under random excitation. Acta Mech Sin 32(5):1–18

Mao Z, Sinnott SB (2000) A computational study of molecular diffusion and dynamic flow through carbon nanotubes. J Phys Chem B 104(19):4618–4624

Mattia D, Calabrò F (2012) Explaining high flow rate of water in carbon nanotubes via solid–liquid molecular interactions. Microfluid Nanofluid 13(1):125–130

Mattia D, Gogotsi Y (2008) Review: static and dynamic behavior of liquids inside carbon nanotubes. Microfluid Nanofluid 5(3):289–305

Meo M, Rossi M (2006) Prediction of Young's modulus of single wall carbon nanotubes by molecular-mechanics based finite element modelling. Compos Sci Technol 66(11):1597–1605

Moore RE (1979) Methods and applications of interval analysis. Society for Industrial and Applied Mathematics, Philadelphia

Narendar S, Gopalakrishnan S (2010) Terahertz wave characteristics of a single-walled carbon nanotube containing a fluid flow using the nonlocal Timoshenko beam model. Physica E 42(5):1706–1712

Narendar S, Gupta SS, Gopalakrishnan S (2012) Wave propagation in single-walled carbon nanotube under longitudinal magnetic field using nonlocal Euler–Bernoulli beam theory. Appl Math Model 36(9):4529–4538

Neumaier A (1990) Interval methods for systems of equations. Cambridge University Press, Cambridge

Rao SS, Berke L (1997) Analysis of uncertain structural systems using interval analysis. AIAA J 35(4):727–735

Ritto TG, Soize C, Rochinha FA, Sampaio R (2014) Dynamic stability of a pipe conveying fluid with an uncertain computational model. J Fluids Struct 49:412–426

Robinson MTA, Adali S (2016) Variational solution for buckling of nonlocal carbon nanotubes under uniformly and triangularly distributed axial loads. Compos Struct 156:101–107

SafarPour H, Ghadiri M (2017) Critical rotational speed, critical velocity of fluid flow and free vibration analysis of a spinning SWCNT conveying viscous fluid. Microfluid Nanofluid 21(2):22

Salvetat JP, Briggs GAD, Bonard JM et al (1999) Elastic and shear moduli of single-walled carbon nanotube ropes. Phys Rev Lett 82(5):944–947

Scarpa F, Adhikari S (2008) Uncertainty modeling of carbon nanotube terahertz oscillators. J NonCryst Solids 354(35):4151–4156

Setoodeh AR, Khosrownejad M, Malekzadeh P (2011) Exact nonlocal solution for postbuckling of single-walled carbon nanotubes. Physica E 43(9):1730–1737

Skoulidas AI, Ackerman DM, Johnson JK, Sholl DS (2002) Rapid transport of gases in carbon nanotubes. Phys Rev Lett 89(18):185901

Sofi A, Muscolino G (2015) Static analysis of Euler–Bernoulli beams with interval Young's modulus. Comput Struct 156:72–82

Sofi A, Muscolino G, Elishakoff I (2015a) Natural frequencies of structures with interval parameters. J Sound Vib 347:79–95

Sofi A, Muscolino G, Elishakoff I (2015b) Static response bounds of Timoshenko beams with spatially varying interval uncertainties. Acta Mech 226(11):3737–3748

Treacy MMJ, Ebbesen TW, Gibson JM (1996) Exceptionally high Young's modulus observed for individual carbon nanotubes. Nature 381:678–680

Tu ZC, Ou-Yang ZC (2002) Single-walled and multiwalled carbon nanotubes viewed as elastic tubes with the effective Young's moduli dependent on layer number. Phys Rev B 65(23):233407

Wang Q, Zhou GY, Lin KC (2006) Scale effect on wave propagation of double-walled carbon nanotubes. Int J Solids Struct 43(20):6071–6084

Wang B, Deng Z, Ouyang H, Zhang K (2013) Wave characteristics of single-walled fluid-conveying carbon nanotubes subjected to multi-physical fields. Physica E 52:97–105

Wang B, Deng Z, Ouyang H, Zhou J (2015) Wave propagation analysis in nonlinear curved single-walled carbon nanotubes based on nonlocal elasticity theory. Physica E 66:283–292

Wong EW, Sheehan PE, Lieber CM (1997) Nanobeam mechanics: elasticity, strength, and toughness of nanorods and nanotubes. Science 277:1971–1975

Xia W, Wang L (2010) Microfluid-induced vibration and stability of structures modeled as microscale pipes conveying fluid based on non-classical Timoshenko beam theory. Microfluid Nanofluid 9(4–5):955–962

Zhang H, Ye H, Zheng Y, Zhang Z (2010) Prediction of the viscosity of water confined in carbon nanotubes. Microfluid Nanofluid 10(2):403–414

Zhen YX, Fang B, Tang Y (2011) Thermal–mechanical vibration and instability analysis of fluid-conveying double walled carbon nanotubes embedded in visco-elastic medium. Physica E 44(2):379–385